Synthesis and Characterization of Diamond-Coated CNTs and Their Reinforcement in Nylon-6 Single Fiber

Vijaya K. Rangari,*,† Ghouse M. Mohammad,† Shaik Jeelani,† Yuri V. Butenko,‡ and Vinod R. Dhanak§

Materials Science and Engineering, Tuskegee University, Tuskegee, Alabama 36088, School of Chemical Engineering and Advanced Materials, University of Newcastle upon Tyne, Newcastle upon Tyne NE1 7RU, United Kingdom, and Physics Department, University of Liverpool, Liverpool L69 3BX, United Kingdom

ABSTRACT Diamond nanoparticle (DN)-coated CNTs were synthesized using a cationic surfactant-assisted sonochemical method. The as-prepared DN coated CNTs were characterized using X-ray diffraction (XRD), X-ray photoelectron spectroscopy (XPS), and transmission electron microscopy (TEM). The results show that the DNs were coated on the outer wall surface of CNTs. The DN-coated CNTs were infused in Nylon-6 polymer through a melt extrusion process to form nanocomposite fibers that were tested for their tensile properties. The ultimate tensile strength is found to be 363 MPa for DN/CNTs/Nylon-6 single fibers as compared to 240 MPa for neat Nylon-6 single fibers. These results were also compared with Nylon-6 fibers infused with pristine CNTs and pristine DNs.

KEYWORDS: CNTs • diamond nanoparticles • Nylon-6 • nanocomposites • fibers

INTRODUCTION

Carbon-based materials such as fullerenes, nanotubes, nanodiamond, nanorods, nanocones, nanowalls etc., with their wide range of stable forms from differently hybridized covalent bonds, are at the front line of the research efforts in nanoscience and technology. Research and fundamental studies on these nanostructured carbon materials have gained tremendous interest among the nanotechnologists after the discovery of the carbon nanotubes (CNTs). Carbon allotropes like diamond and nanotubes (CNTs), despite having different carbon−carbon bonds, are high-strength materials (1). Diamond nanoparticles have aroused considerable interest because of their ability to resist pressure and permanent deformation, and their high scratch resistance. It is generally accepted that diamond nanoparticles (DN) consist of facets less than 100 nm in size (2). From the smallest diamondoids (adamantane and the higher diamondoids) (3) to the larger grain size films and particles there exists a plethora of sizes of particles and films with different morphology, sp^2 content and hydrogen incorporation. Diamond nanoparticle (DN) films are expected to possess the superior properties of diamond combined with smooth surfaces and low stress (4). The use of nanocrystalline diamond powders for industrial applications such as abrasives, hard coatings, and cutting materials is a particularly attractive prospect because of isomorphic shapes of these diamonds compared to larger microcrystalline diamond powders. The application of nanodiamond in the development of very hard metal composites is evidence of the advantages in hardness, weight, and wear resistance. Although diamond thin films are already widely used in industry as wear-resistant coatings because of their extreme hardness (bulk hardness >80 GPa), they are often quite brittle as a result of their low fracture toughness (KIC ∼5 MPa, (m) 1/2). On the other hand, the exceptional properties of carbon nanotubes (CNTs) such as high tensile strength, excellent radial elastic deformability and extreme toughness have paved way for their use in the next generation composite materials (5, 6). Furthermore, unlike diamond, CNTs are conducting. Because of the unique hardness of diamond and the tensile strength of CNTs, it is not unreasonable to expect that a composite, combining CNTs and diamond, to have unique mechanical properties (7). Diamond/CNTs composites may thus find applications in various fields that require a combination of good mechanical, thermal and electrical properties such as wear-resistant coatings, thermal management of integrated circuits (ICs), polymer fabrics, and composites. It is believed that the combination of CNTs and nanodiamond, diamond like carbon (DLC) or graphene could be used in applications of electronic devices, biodevices and micro- and nanoelectromechanical systems. Nanodiamond and diamond-like carbon are intended to provide a hard, scratch-resistant, transparent, hermetic, corrosion-resistant, and electrically insulating coating for CNTs. One of the means to modify CNTs by diamond nanoparticles is to attach the diamond nanomaterials noncovalently, such as by means of van der Waals forces (8). Sonochemical

* Corresponding author. E-mail: rangariv@tuskegee.edu. Fax: 1334-724-4875.
Received for review October 19, 2009 and accepted June 07, 2010
† Tuskegee University.
‡ University of Newcastle upon Tyne.
§ University of Liverpool.
DOI: 10.1021/am1002926

ARTICLE

synthesis has also proven to be a useful technique to generate core/shell-type nanomaterials (9). The chemical effects of ultrasound arise from acoustic cavitations involving the formation, growth, and collapse of bubbles in liquid, which generates localized hot spots having a temperature of roughly 5000 K, pressure of about 20 MPa, and very high cooling rates of about 1×10^7 Ks (10−13). These extreme conditions can drive chemical reactions such as oxidation, reduction, dissolution, dispersion of nanoparticles, and surface area increase and can be achieved using ultrasound irradiation (14).

The cavitation in liquid and solid systems produces mechanochemical effects, in addition to the homogeneous cavitation observed in pure liquids. The damage associated with jet formation cannot occur if the solid particles are smaller than the collapsing bubble size (15, 16). In these cases, the shock waves created by homogeneous cavitation, however, can create high velocity interparticle collisions. The cavitation and shockwaves in slurry can accelerate solid particles to high velocities and the resultant collisions are capable of inducing dramatic changes in surface morphology, composition, and reactivity (10). Agglomeration of metal powders, fragmentation of brittle solids, enhancement of the reactivity of metals, enhancement of rates of intercalation in layered materials, and enhancement of the rates of catalytic reactions are some of the observed mechanochemical effects of ultrasound (10).

In this study, DN-coated CNTs were synthesized using sonochemical technique in the presence of cationic surfactant CTAB. These hybrid nanoparticles were characterized using XRD, XPS, and TEM analysis. The nanoparticles were then were then introduced into Nylon-6 polymer through a melt extrusion process and the resulting single fibers were tested for their tensile and thermal properties.

EXPERIMENTAL SECTION

Synthesis of DN-Coated CNTs. Multiwalled carbon nanotubes (CNTs) used in this study were purchased from Nanostructured & Amorphous Materials. These CNTs are <95% pure (stock #1205YJ) with a density of 0.04−0.05 g/cm^3, 10−20 nm in diameter and ∼15 μm in length. The detonation DN used in this research was provided by the Lavrentiev Institute of Hydrodynamics (from the Siberian Branch of Russian Academy of Sciences, Novosibirsk, Russia) (14). The samples were cleaned in a mixture of $HClO_4$ and H_2SO_4 acids and washed with hydrochloric acid and distilled water (17). The diamond fraction in the sample was approximately 86% (17). The size distribution of DN particles in the sample varied from 2−20 nm with an average particle size of 4−5 nm as determined previously (18). Five-hundred milligrams of CNTs was added to ∼60 mL of dimethylformamide solution and magnetically stirred for about half an hour using a magnetic stirrer to deagglomerate CNTS and form a uniformly dispersed solution. Two-hundred-fifty milligrams of DN and 500 mg of CTAB (Cetyltrimethyl Ammonium Bromide, Sigma-aldrich) surfactant were then added to the solution and stirred again for another half an hour to obtain a uniform dispersed solution. This reaction mixture is irradiated with a high intensity Sonics Vibra Cell Ultrasonic Liquid Processor (Ti-horn, 20 kHz, 100W/cm2) at 50% of amplitude for 3 h. To avoid a temperature increase during the sonication process, we employed external cooling by circulating cooled liquid (kept at 10 °C by a thermostate control) through a jacketed reaction vessel for the entire period of reaction time. The reaction product was later washed with ethanol and centrifuged at 12 000 rpm at 12 °C for about 10 min to separate the nanoparticles from the solution. The procedure was repeated 4−5 times to remove any excess surfactant. The residue was then dried under a vacuum at room temperature. The as-prepared DN -coated CNTS were then characterized using X-ray diffraction (XRD), X-ray photoemission spectroscopy (XPS), and transmission electron microscopy (TEM) analysis. XPS measurements, using the ESCA300 spectrometer at NCESS in the UK (17−21), was used to confirm the presence of DN in the DN-coated CNTs while the XRD study, using a Rigaku D/MAX 2200 X-ray diffractometer, was used to investigate the crystalline nature of the DN-CNTs nanoparticles. TEM, using (JEOL-2010), was used to examine the morphology and size of the DN-CNTs.

Fabrication of Nylon-6 Composite Single Fibers. Commercial grade UBE Nylon P1011F (Nylon-6, commercial name-Polyamide 6) was procured from UBE America, Inc. The density of Nylon-6 is 1.09−1.19 g/cm^3, whereas the melting point is around 115−250 °C. The nanoparticles and Nylon-6 powder were carefully measured in the ratio of 1:99 by weight and noncontact dry mixing of DN-CNTs/Nylon-6, DN/Nylon-6 or CNTs/Nylon-6 powder were carried out using the dual centrifugal Thinky machine running at 2000 rpm for about 10 min. This procedure was repeated for 5−6 times to achieve a uniform color of the mixture. The dry powder mixture of nanoparticles and Nylon-6 polymer powders were dry mixed one more time using a hoper connected to the hot air dryer for another 24 h and extruded directly without exposing to the air using a Wayne.

Yellow-Label Table-Top Extruder. The extruder has a 19 mm diameter screw, which is driven by a 2HP motor. Thermostatically controlled five heating zones were used to melt the mixture before extrusion of single fiber, three inside the barrel and two in the die zone at set temperatures of 226, 235, 243, 246.1, and 248.8 °C, respectively. Nylon-6 starts melting because of high barrel temperature and CNTs are randomly distributed within the liquid matrix. The screw rotation induces the high velocity liquid to experiences enormous shear force. The shear force contributes to the orientation of CNTs (19, 20). The die configuration generates two distinct flow regimes that highly affect the fiber alignments. First, the converging die inlet introduces a converging flow pattern, which in turn aligns the fibers along the streamline direction. Second, the narrow orifice allows the flow pattern to transform into shear flow as it enters the narrow orifice. The shear flow produces additional fiber alignment due to differential shear rate along the boundary layer that orients the fibers in the direction of flow. This is a continuous process and the composite filaments with constant tension were extruded at a screw speed of 10 rpm and feed rate of approximately 80 g/h. The filaments were stabilized by using a setup of two godet machines and were finally wound on a spool using Wayne desktop filament winder at a winding speed of 50 rpm. Four sets of extrusions were carried out to obtain single fibers of (a) neat Nylon-6, (b) CNTs-infused Nylon-6, (c) DN-infused Nylon-6, and (d) DN-coated CNT-infused Nylon-6. Tensile tests on the single fibers of each of the four samples were conducted on a Zwick Roell tensile tester equipped with a 20 N Load Cell. The tests were run under displacement control at a crosshead speed of 0.01 1/s strain rate and gage length of 102 mm.

RESULTS AND DISCUSSION

Characterization of DN-Coated CNTs. X-ray photoemission spectroscopy (XPS) was used to confirm the presence of DN in the DN-coated CNTs. The XPS measurements were done using the ESCA300 spectrometer at NCESS in the U.K. (21, 29). A thin layer of each of the powder

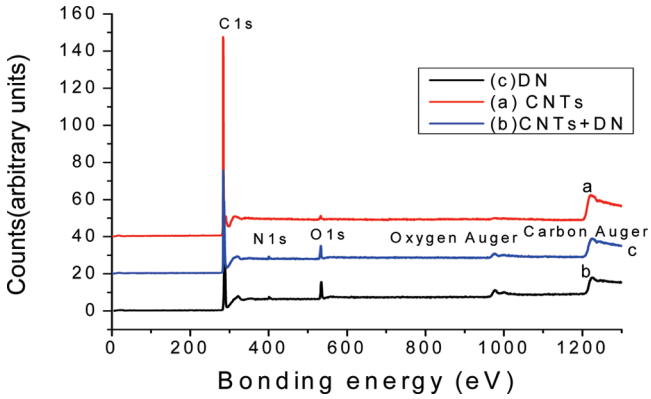

FIGURE 1. XPS survey spectra from pristine MWNT, DN, and DN-coated MWNT

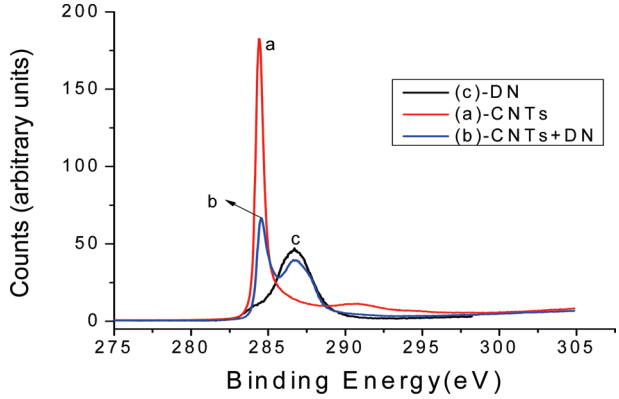

FIGURE 2. C1s XPS spectra from pristine CNTs, DN, and DN-coated CNTs

samples of pristine CNTs and DN-coated CNTs was mounted on a standard stainless steel sample stub using double-sided adhesive tape. Spectra were recorded at an electron takeoff angle of 45 degrees. Charge compensation was achieved using a VG Scienta FG300 low-energy electron flood gun with the gun settings adjusted for optimum spectral resolution. For the current samples, it was found that zero bias was adequate to get the spectra for the samples containing CNTs. This is because pristine CNTs are conducting. Although DN itself is not conducting, the presence of the conducting CNTs in the DN-coated samples was sufficient so as not to require charge compensation. For the pristine as-received DN, charge compensation of about 5 V was applied. The X-ray source power was 2.8 kW and the spectrometer pass energy was 150 eV with the entrance-slit width of the hemispherical analyzer set to 1.9 mm. Under these conditions, the overall spectrometer resolution was about 0.5 eV.

XPS survey scans of the pristine as received CNTs, DN, and DN-coated CNTs are presented in Figure 1, showing peaks mainly due to carbon. There is a small peak due to oxygen, which is usually present in the as-received samples, due to oxidation or attachment of oxygen containing species at CNTs and DN defect sites. The DN and DN-coated CNTs also show the presence of nitrogen, which is absent in the pristine CNTs spectrum. Figure 2 compares the C1s spectra from the CNTs, DN, and DN-coated CNT samples. A single peak at about 284.5 eV binding energy characterizes the CNTs and a broad feature at about 290 eV related to shakeup

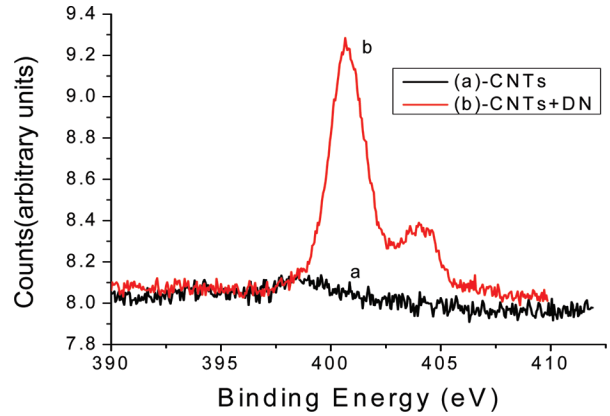

FIGURE 3. N1s XPS spectra from pristine CNTs and DN-coated CNTs.

loss effects. This C1s line shape is typical of sp^2-bonded graphitic type carbon that makes up the CNTs. The C1s spectrum from the pristine DN is characterized by a single peak at about 286.8 eV together with a broadening toward lower binding energy and a small shoulder at about 284.5 eV. These features from DN are typical of as-received samples because the material consists of a trace of sp2 bonded graphitic carbon impurity. The presence of DN in the DN-coated CNTs is shown by the appearance of a second broader peak centered at about 286.8 eV in addition to the peak due to CNTs at 284.5 eV. The peak at 286.8 eV is due to sp^3-bonded carbon in the DN (18). This peak is not as sharp as the one due to the carbon in CNTs and reflects possible effects due to nonuniformity in the size distribution of the DN (18).

Additional confirmation of the presence of DN in the CNTs is shown in Figure 3, which compares the XPS of N1s in the CNTs and DN-CNTs. In the pristine CNTs, there is no presence of nitrogen. In the DN-CNT case, the figure shows the presence of two peaks in the N1s spectrum, centered at 400.7 eV and a smaller peak at 404.2 eV, and is similar to what has been observed previously from pristine detonation DN (18). The XPS spectra from pristine DN have been discussed in detail in ref 18. The presence of nitrogen in the DN has been accounted for by the presence of this element in the initial explosive mixture (30−33) and its incorporation into the diamond lattice during the detonation synthesis. Clearly, there are two forms of nitrogen-containing species in the DN. According to ref 18, it is believed the first one at 400.7 eV could belong to substitutional nitrogen atoms having three neighboring carbon atoms. The second peak at 404 eV has been ascribed to trapped molecular nitrogen in the diamond lattice.

The XRD patterns of as-prepared DN-CNT, diamond, and CNT nanoparticles are presented in Figure 4. These XRD results shows that the CNTs and DN are highly crystalline in nature and all the peaks match very well with JCPDS of graphitic carbon (26−1077) and diamond (06−0675), respectively. It should be noted that the peak intensities of CNTs (~26.3° 2θ) decrease after coating with DN nanoparticles. Similar results were observed by other researchers (22, 23) in the case of iron-oxide-coated CNTs. The crystallite

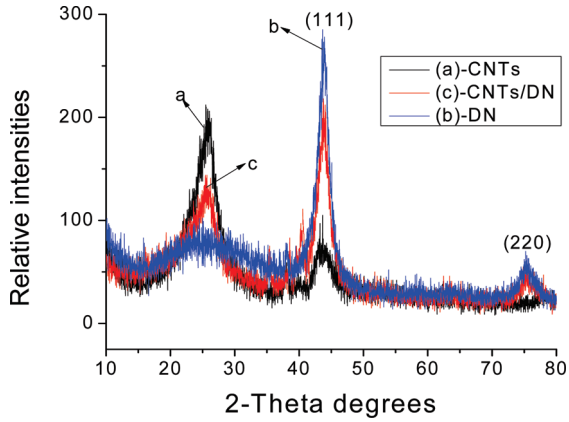

FIGURE 4. XRD pattern of (a) CNTs nanoparticles, (b) DN nanoparticles, and (c) DN-CNTs.

particle sizes for as-received DN and DN coated on CNTs were calculated using the Debye−Scherrer equation (24). The fwhm (full width half maxima) measured from XRD for DN at angle 43.659 and DN coated CNTs at angle 43.793 are 0.737 and 1.180, respectively. The crystallite sizes calculated from these fwhm's are 11.6 and 7.3 nm for as-received DN and DN coated CNTs, respectively. These results are consistent with the TEM results (see below) and the supplier's specifications. The X-ray diffraction peak broadening can be primarily observed because of the size of the nanoparticles and also can be due to strain or defects in the crystalline material. As discussed above, the peak broadening is more (1.180) for DN-coated CNTs than the DN (0.737). This may be because of the DN coated on CNTs are strained.

TEM studies were carried out to understand the extent of DN coating on CNTs. Images a and b in Figure 5 shows the TEM picture of DN coated on CNTs at two different magnifications. These micrographs clearly show that the DNs are coated on the outer wall surface of CNTs. The diamond nanoparticle sizes in images a and b in Figure 5 measure ~5 nm in diameter and CNTs are about 10 nm in diameter. The measured size of the ND is consistent with what has been previously reported for the as supplied ND (18). All the micrographs showed that there was no presence of free ND detached from the walls of the CNTs. Figure 5c presents a high-resolution micrograph of one of the DN from the DN-coated CNTs, showing the lattice spacing's of the (111) planes of diamond. The crystals with an average *d*-spacing of 0.21 nm confirms the presence of diamond (25). A selected area diffraction pattern form DN coated CNTs are shown in Figure 5d, further confirming the crystal-

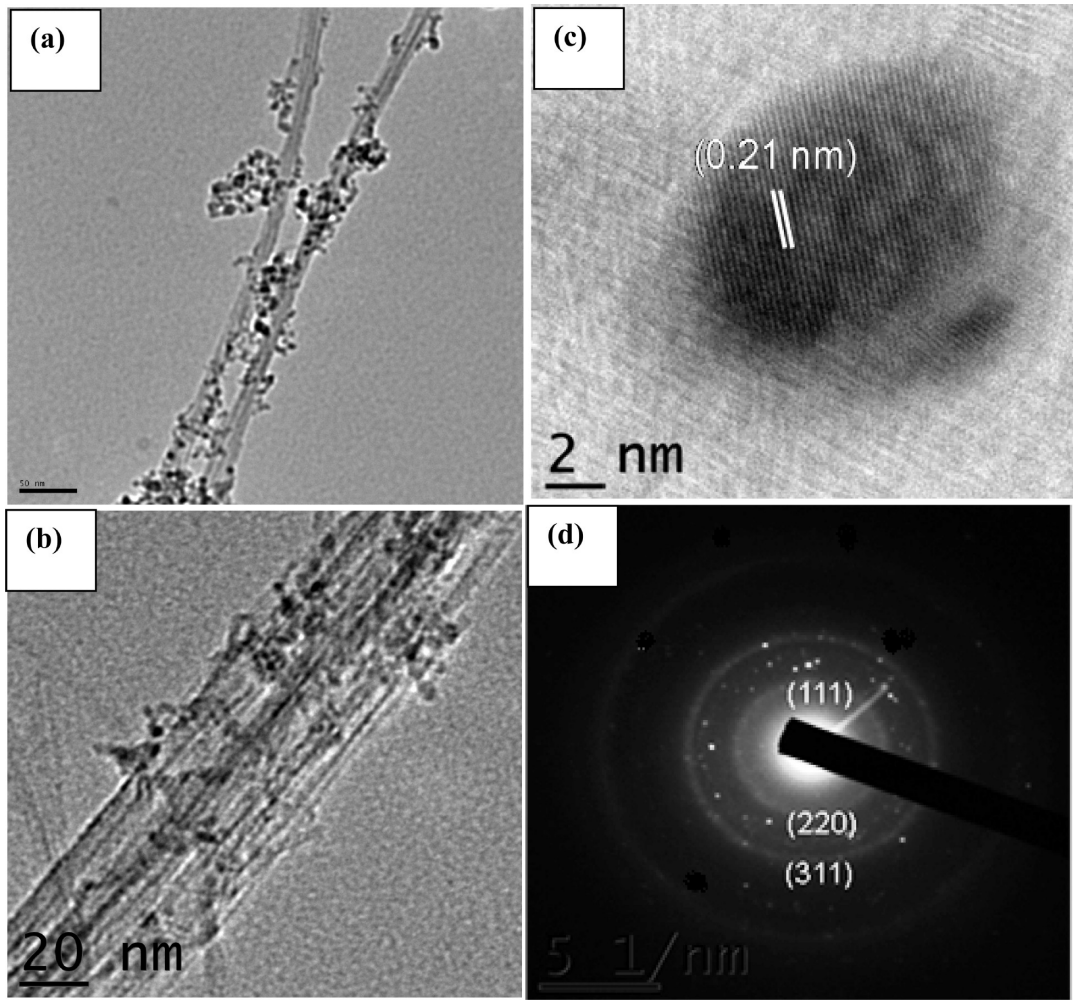

FIGURE 5. TEM- micrograph of (a) DN nanoparticles coated on CNTs at 50 nm scale bar, (b) DN nanoparticles coated on CNTs at 20 nm scale bar, (c) DN nanoparticle (111) lattice on CNTs. (d) Electron diffraction of DN coated on CNTs.

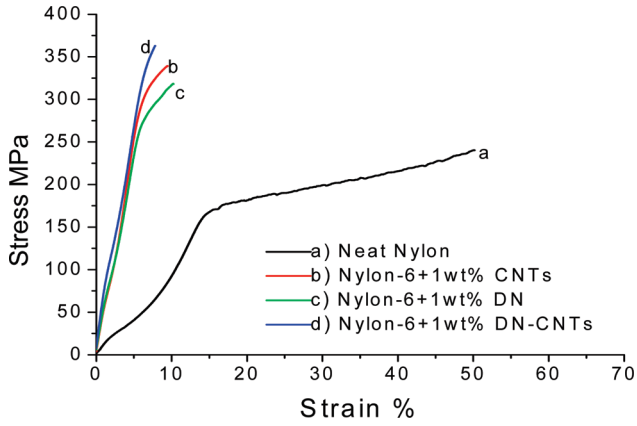

FIGURE 6. Tensile response of (a) neat Nylon-6, (b) CNT-Nylon-6, (c) DN-Nylon-6, and (d) DN-CNT-Nylon-6 fibers.

line quality of the DN on CNTs (26). It is worth mentioning that the reciprocal space position scale is not corresponding to the diffraction rings.

It is possible that the solvent DMF and CTAB cationic surfactant play a role in the attachment of the DN to the outer wall of the CNTs, although the mechanism for this is not clear. The DMF appears to play an important role in the initial debundling of CNTs and separation into individual single CNTs. It is possible that DMF cationic surfactant molecules initially adsorb onto the CNTs, weakening the van der Waals attraction between the CNTs. In a second step, the addition of CTAB to the CNTs/DMF mixture creates a uniform coating of CTAB molecules on CNTs. Finally, the ultrasound irradiation of DN in the presence of CNTs/CTAB/DMF reaction mixture results in a coating of DN on CNTs. The ratio of CNTs to DN nanoparticles (2:1 by weight) mixture that we use in this study is optimum, because we find that higher ratio of CNTs to DN nanoparticles leaves free DN in the mixture, whereas a lower ratio leaves larger areas of CNTs uncoated.

The ultrasound irradiation is known for creating extreme mechanical effects by producing shock waves, liquid jet and acoustic streaming (27, 28). In our case, possibly the shock wave produced by the implosion of cavitations, bubble in DMF is responsible for this coating of DN on CNTs.

Tensile Response. Tensile tests of single-fiber specimens of the Nylon-6 composites infused with 1 wt % CNTS, 1 wt % DN, and 1 wt % DN-coated CNTs were carried out to estimate the increase in mechanical properties, such as strength and modulus. The tests were performed using a Zwick/Roell single filament testing equipment according to the ASTM standard D 3379−75 (34). Figure 6 compares the stress versus strain curves for the four samples and the parameters extracted from the data are summarized in Table 1.

The data show that the ultimate tensile strength for the CNTs infused Nylon-6 is higher than that of the neat Nylon-6 fibers, in agreement with our previous measurements. On the other hand, the performance of Nylon-6 infused with just DN, although better than neat Nylon-6, does not improve on the Nylon-6 with CNTs. This probably reflects on the fact that CNTs align themselves along the polymer chains, unlike the "spherical" DNs. Nylon-6 with the DN coated CNTs are found to have the most improvement of all the samples although it is noted that the strain to fracture values are compromised. This appears to be the trend, as the tensile strength improves by the addition of the carbon nanoparticles, the strain to fracture ratio goes down. The tensile strength and modulus of the Nylon-6 infused with DN-coated CNTs is 51 and 698 % higher than the neat Nylon-6 polymer fibers. It can be seen from Figure 6 that the 1 wt % DN-coated CNTs infused Nylon-6 fibers are very hard and brittle and their modulus is the highest (6.7 GPa). This measured strength value for nanocomposite fiber is more than 50 % higher than that of the neat Nylon-6, which indicates the high load-bearing capability of DN-coated CNTs and their potential applications in structural composite materials for various applications. The significant improvement of tensile modulus can be attributed to the infusion of high strength DN/CNTs, their alignment in extrusion direction of Nylon-6 polymer fibers. Similar improvements have been observed in our earlier experiments (19, 20, 34). We have also tried to coated higher percentage of DN on CNTs but we have observed most of the DN are free and isolated rather than on the surface of CNTs. That is the reason we have not extruded these in to fibers. As for the amount used for infusion into the Nylon-6, in our experience, we find that it is difficult to extrude fibers if we use more than 1 wt % of CNTs or DN on CNTs, as the nanoparticles tend to agglomerate and break the fiber.

CONCLUSIONS

In summary, a sonochemical synthesis technique has been developed to coat DN nanoparticles on CNTs. These DN-coated CNTs were characterized using XPS, XRD, and TEM. The spectroscopic results show the presence of DN in the DN-coated CNTs. TEM results clearly show the DNs are coated on the outer surface of CNTs and XRD results also confirm the presence of DN on CNTs. The ratio of CNTs to DN nanoparticles (2:1 by weight) mixture that we use in this study is optimum, because we find that a higher ratio of CNTs to DN nanoparticles leaves free DN in the mixture, whereas a lower ratio leaves larger areas of CNTs uncoated. These DN coated on CNTs were infused in Nylon-6 polymer fibers through an extrusion process to alignment/disperse

Table 1. Tensile Property Data for Neat Nylon-6 and Nanocomposite Fibers Filled with CNTs, DN, and DN-Coated CNTs

sample fiber	tensile strength (MPa)	Δ %	tensile modulus (GPa)	Δ %	elongation %
neat Nylon-6	240 ± 5		0.84 ± 0.1		50.0 ± 0.3
1.0 wt % CNTs/Nylon-6	339 ± 4	41	5.05 ± 0.3	501	9.4 ± 0.5
1.0 wt % DN/Nylon-6	319 ± 6	32	5.14 ± 0.2	512	10.2 ± 0.2
1.0 wt % DN-coated CNTs/Nylon-6	363 ± 2	51	6.7 ± 0.1	698	7.8 ± 0.1

the nanoparticles to improve the mechanical properties. The tensile properties of these fibers show that the DN-coated-CNT-infused Nylon-6 fibers can take 51% more load than the neat Nylon-6 fibers. Nylon-6 with DN-coated CNTs also shows improvements in mechanical properties compared to Nylon-6 infused with just CNTs or just DNs. As for the amount used for infusion into the Nylon-6, in our experience, we find that it is difficult to extrude fibers if we use more than 1 wt % CNTs or DN on CNTs, as the nanoparticles tend to agglomerate and break the fiber.

Acknowledgment. The authors thank the National Science Foundation for its financial support through NSF-PREM and NSF-RISE grants.

REFERENCES AND NOTES

(1) Fernandes, A. J. S.; Pinto, M.; Neto, M. A.; Oliveira, F. J.; Silva, R. F.; Costa, F. M. *Diamond Relat. Mater.* **2009**, *18*, 160–163.
(2) Williams, O. A.; Nesladek, M.; Daenen, M. *Diamond Relat. Mater.* **2008**, *17*, 1080–1088.
(3) Dahl, J. E.; Liu, S. G.; Carlson, R. M. K. *Science* **2003**, *299*, 96–99.
(4) Field, J. E. *The Properties of Diamond*; Academic Press: London, 1979.
(5) Ajayan, P. M.; Schadler, L. S.; Giannaris, C.; Rubio, A. *Adv. Mater.* **2000**, *12*, 750–753.
(6) Thostenson, E. T.; Ren, Z.; Chou, T. W. *Compos. Sci. Technol.* **2001**, *61*, 1899–1912.
(7) Shankar, N.; Gulmac, N. G.; Yu, M. F.; Vanka, S. P. *Diamond Relat. Mater.* **2008**, *17*, 79–83.
(8) Li, Q.; Ni, N.; Gong, J.; Zhu, D.; Zhu, Z. *Carbon* **2008**, *46*, 434–439.
(9) Shu, F. W.; Feng, G.; Meng, K. L.; Guang, J. Z.; Ai, Y. Z. *J. Cryst. Growth* **2006**, *289*, 621–625.
(10) Suslick, K. S.; Choe, S. B.; Cichowlas, A. A.; Grinstaff, M. W. *Nature* **1991**, *353*, 414–416.
(11) Suslick, K. S.; Hammerton, D. A.; Cline, R. E. *J. Am. Chem. Soc.* **1986**, *108*, 5641–5642.
(12) Xu, S.; Wang, H.; Zhu, J. J.; Xin, X. Q.; Chen, H. Y. *Eur. J. Inorg. Chem.* **2004**, *23*, 4653–4659.
(13) Xia, X. H.; Luo, Y. S.; Wang, Z.; Liang, Y.; Fan, J.; Jia, Z. J.; Chen, Z. H. *Mater. Lett.* **2007**, *61*, 2571–2574.
(14) Liamkin, I.; Petrov, E. A.; Ershov, A. P.; Sakovich, G. V.; Staver, A. M.; Titov, V. M.; Dokl, A. *Nauk SSSR* **1988**, *302*, 611–613.
(15) Barber, B. P.; Putterman, S. J. *Phys. Rev. Lett.* **1992**, *69*, 1182–1184.
(16) *Ultrasound: Its Chemical, Physical, and Biological Effects*; Suslick, K. S., Ed.; VCH Publishers: New York, 1988.
(17) Butenko, Y. V.; Kuznetsov, V. L.; Chuvilin, A. L.; Kolomiichuk, V. N.; Stankus, S. V.; Khairulin, R. A.; Segall, B. *J. Appl. Phys.* **2000**, *88*, 4380–4388.
(18) Yeganeh, M.; Coxon, P. R.; Brieva, A. C.; Dhanak, V. R.; Siller, L.; Butenko, Y. V. *Phys. Rev. B* **2007**, *75*, 155404–155412.
(19) Rangari, V. K.; Mohammad, Y.; Mahfuz, H.; Jeelani, S. *Mater. Sci. Eng., A.* **2009**, *500*, 92–97.
(20) Mahfuz, H.; Adnan, A.; Rangari, V. K.; Jeelani, S. *Int. J. Nanosci.* **2005**, *4*, 55–72.
(21) Beamson, G. ; Briggs, D. *High-Resolution XPS of Organic Polymers: The Scienta ESCA300 Database*; John Wiley & Sons: New York, 1992.
(22) Huiqun, C.; Meifang, Z.; Yaogang, L. *J. Solid State Chem.* **2006**, *179*, 1208.
(23) Wanda, D. ; Rangari, V. K. ; Tarig, A. H. ; Jeelani, S. J. Appl. Polym. Sci., 2010, 10.1002/app.31193
(24) Klug, H.; Alexander, L.; *X-ray Diffraction Procedures*; Wiley: New York, 1962; p. 125.
(25) *ICDD Diffraction Database PDF 2206−0675*; International Centre Diffraction Data: Newtown Square, PA.
(26) Li, Y. B.; Zhu, Y. Q.; Gao, G. D.; Liang, J.; Wei, B. Q.; Wu, D. H.; Hui, M. J. *J. Mater. Sci. Lett* **1995**, *14*, 1281.
(27) Dahlem, O.; Demaiffe, V.; Halloin, V.; Reisse, J. *AIChE J.* **1998**, *44*, 2724–2730.
(28) Doktyecz, S. J.; Suslick, K. S. *Science* **1990**, *247*, 1067–1069.
(29) Beamson, G.; Briggs, D.; Davies, S. F.; Fletcher, I. W.; Clark, D. T.; Howard, J.; Gelius, U.; Wannberg, B.; Balzer, P. *Surf. Interface Anal.* **1990**, *15*, 541–549.
(30) Staver, A. M.; Gubareva, N. V.; Lyamkin, A. I.; Petrov, E. A. *Combust. Explos. Shock Waves.* **1984**, *20*, 567–569.
(31) Greiner, N. R.; Phillips, D. S.; Johnson, J. D.; Volk, F. *Nature* **1990**, *333*, 440–442.
(32) Shenderova, O. A.; Gruen, D. M. *Ultrananocrystalline Diamond: Synthesis, Properties and Applications*; William Andrew Publishing: New York, 2006.
(33) Kuznetsov, V. L.; Chuvilin, A. L.; Moroz, E. M.; Kolomiichuk, V. K.; Shaichutdinov, S. K.; Butenko, Y. V.; Malkov, I. Y. *Carbon* **1994**, *32*, 873–882.
(34) Rangari, V. K.; Yousuf, M.; Jeelani, S.; Pulikkathara, M. X.; Khabashesku, V. N. *Nanotechnology* **2008**, *19*, 245703–245712.

AM1002926